The Meteoritical Society

*Meteoritics & Planetary Science* 50, Nr 5, 944–957 (2015)
doi: 10.1111/maps.12441

# From olivine to ringwoodite: a TEM study of a complex process

Lidia PITTARELLO[1*], Gang JI[2,5], Akira YAMAGUCHI[3], Dominique SCHRYVERS[2], Vinciane DEBAILLE[4], and Philippe CLAEYS[1]

[1]Analytical, Environmental and Geo-Chemistry (AMGC), Earth System Science, Vrije Universiteit Brussel, Pleinlaan 2, 1050 Brussels, Belgium
[2]Electron Microscopy for Materials Science (EMAT), University of Antwerp, Groenenborgerlaan 171, 2020 Antwerp, Belgium
[3]National Institute of Polar Research, 10-3 Midori-cho, Tachikawa, Tokyo 190-8518, Japan
[4]Laboratoire G-Time (Géochimie: Tracage isotopique, minéralogique et élémentaire), Université Libre de Bruxelles, Av. F.D. Roosevelt 50, 1050 Brussels, Belgium
[5]Present address: Unité Matériaux et Transformations, UMR CNRS 8207, Bâtiment C6, Université Lille 1, 59655 Villeneuve d'Ascq Cedex, France
[*]Corresponding author. E-mail: lidia.pittarello@vub.ac.be

*(Received 13 November 2014; revision accepted 02 February 2015)*

**Abstract**–The study of shock metamorphism of olivine might help to constrain impact events in the history of meteorites. Although shock features in olivine are well known, so far, there are processes that are not yet completely understood. In shock veins, olivine clasts with a complex structure, with a ringwoodite rim and a dense network of lamellae of unidentified nature in the core, have been reported in the literature. A highly shocked (S5-6), L6 meteorite, Asuka 09584, which was recently collected in Antarctica by a Belgian–Japanese joint expedition, contains this type of shocked olivine clasts and has been, therefore, selected for detailed investigations of these features by transmission electron microscopy (TEM). Petrographic, geochemical, and crystallographic studies showed that the rim of these shocked clasts consists of an aggregate of nanocrystals of ringwoodite, with lower Mg/Fe ratio than the unshocked olivine. The clast's core consists of an aggregate of iso-oriented grains of olivine and wadsleyite, with higher Mg/Fe ratio than the unshocked olivine. This aggregate is crosscut by veinlets of nanocrystals of olivine, with extremely low Mg/Fe ratio. The formation of the ringwoodite rim is likely due to solid-state, diffusion-controlled, transformation from olivine under high-temperature conditions. The aggregate of iso-oriented olivine and wadsleyite crystals is interpreted to have formed also by a solid-state process, likely by coherent intracrystalline nucleation. Following the compression, shock release is believed to have caused opening of cracks and fractures in olivine and formation of olivine melt, which has lately crystallized under postshock equilibrium pressure conditions as olivine.

## INTRODUCTION

The evaluation of the shock-metamorphic stage of ordinary chondrites is part of the standard meteorite classification (Stöffler et al. 1991). In particular, the shock metamorphism of olivine, a common phase in meteorites and with a simpler structure than pyroxene, has been extensively studied. Typical shock features of olivine include, with increasing shock pressure, (i) planar fractures (PF); (ii) planar deformation features (PDF); (iii) transition to high-pressure polymorphs, such as wadsleyite and ringwoodite; and (iv) melting (see Madon and Poirier 1983; for pioneering transmission electron microscopy [TEM] studies and Stöffler et al. [1991] and references therein for peak pressure correlation). The shock-metamorphic effects in olivine provide a shock-barometer that reaches higher shock peak pressure than the one based on quartz for terrestrial rocks (as silica is completely molten above 50 GPa, whereas olivine becomes glass only at ~75 GPa; Stöffler and Langenhorst 1994; Langenhorst 2002). High-pressure polymorphs of olivine and pyroxene are commonly observed in shock veins crosscutting ordinary chondrites (e.g., Stöffler and Langenhorst 1994).

© The Meteoritical Society, 2015.

The occurrence of a ringwoodite rim around shocked olivine clasts in shock veins in a L5-6 Antarctic ordinary chondrite, Grove Mountains 052049, has been recently reported by Feng et al. (2011). Xie et al. (2012) further investigated the same sample, finding that the ringwoodite rim is rich in Fe with respect to the original olivine and consists of an aggregate of microcrystals, ~500 nm in size. Stacking faults in ringwoodite and in shocked olivine crystals were observed with TEM by Madon and Poirier (1983) and Miyahara et al. (2008) and related to martensitic transformation and structural stress in crystallization of a fine-grained aggregate of ringwoodite and wadsleyite, respectively. The olivine core of the clasts seems to consist of lamellae of different compositions, which were described also by Walton (2013). Ringwoodite lamellae have been reported to grow in shocked olivine in the wall rock, along the margin of shock veins, and referred to a combination of shock and shear stress (Chen et al. 2004; Greshake et al. 2011). Shocked olivine clasts were investigated also by Miyahara et al. (2008, 2010), who described aggregates of ringwoodite and wadsleyite and layered crystals with wadsleyite core and thin ringwoodite rim newly crystallized from the impact melt.

There are different hypotheses on the formation of the ringwoodite rim and the development of shock lamellae at the core of the clasts. The most accredited are

1. *Solid-state transformation* due to diffusion-controlled growth. This was first theorized by Kerschhofer et al. (1998) and later supported by observations by Chen et al. (2004), Xie et al. (2012), and Walton (2013). The diffusion rate is extremely high because of shock-induced, high-temperature conditions. This explains the different Mg/Fe ratio between ringwoodite and olivine. Kerschhofer et al. (1998) proposed *coherent intracrystalline nucleation* for the formation of ringwoodite along stacking faults in olivine and of wadsleyite in ringwoodite grains, and *incoherent grain boundary nucleation* for the ringwoodite rim that forms around olivine large grains. Heterogeneous nucleation for the formation of ringwoodite grains in the melt was invoked for the formation of individual grains of ringwoodite in the shock melt (Walton 2013). According to Sharp and DeCarli (2006), the formation of ringwoodite in highly shocked chondrites occurs by "reconstructive phase transition," i.e., by nucleation and growth. The growth of ringwoodite is controlled by diffusion if a change in composition is observed or alternatively is controlled by the interface where the ringwoodite nucleates (no change in composition) for coherent intracrystalline nucleation.
2. *Fractional crystallization* of olivine melt. Miyahara et al. (2008) observed zoned olivine clasts in impact melt. The core is $Fa_{24\text{-}26}$, a thin rim is $Fa_{6\text{-}10}$ and consists of wadsleyite, and an outer rim of ringwoodite has the composition $Fa_{28\text{-}38}$. These authors suggested that this was the result of fractional crystallization from a melt of olivine composition, according to temperature–composition phase diagrams. The composition of the core and of the wadsleyite rim did not change during the following evolution, because it was "protected" by the ringwoodite rim. The ringwoodite rim, in contact with the shock melt, on the other hand, has the opportunity to react with the melt, adjusting its composition.

A series (A 09578 - A 09607) of L6 ordinary chondrites, recently collected in Antarctica during a joint Japanese–Belgian expedition, has recorded high shock (Yamaguchi et al. 2014). Shock veins crosscut all the samples and ringwoodite and maskelynite are commonly found. The shock stage therefore corresponds to S5–6, according to the classification by Stöffler et al. (1991). Scanning electron microscopy of shock veins has revealed the occurrence of ringwoodite rimming olivine clasts in the shock veins and the presence of complex features at the core of these clasts, similar to those described by Xie et al. (2012). Here, we present a detail investigation of these shock features by microprobe and transmission electron microscopy. Results are discussed according to the current hypothesis for the formation of these shock features and a comprehensive interpretation is finally proposed.

## METHODS

A 35 μm thick, polished thin section for optical and electron microscopy has been prepared at the National Institute of Polar Research (NIPR), Tachikawa, Japan. Scanning electron microscopy has been done at the Royal Belgian Institute of Natural Science (RBINS), Brussels, Belgium, with a FEI Inspect S50 instrument, equipped with an energy-dispersive spectrometry (EDS) detector. Experimental conditions were 10 mm of minimum working distance, 15 kV acceleration voltage, ca. 300 pA beam current, and 4–6 μm of spot size.

Quantitative analysis of the composition of the investigated phases has been evaluated with a JEOL JXA-8200 electron microprobe, equipped with five wavelength-dispersive spectrometers (WDS) and one EDS, at the NIPR. Operative conditions were 15 kV acceleration voltage, 12 nA beam current, and with a fully focused beam. The ZAF corrections were applied. Detection limit for major elements are: <0.02% for Si, <0.02% for Ti, <0.01% for Al, <0.02% for Cr, <0.03%

Table 1. Composition and crystallographic data of ringwoodite, olivine, and wadsleyite phases (after Smyth and Bish 1988).

| Phase | Formula | Crystal system | Lattice parameters (Å) | Space group |
|---|---|---|---|---|
| Olivine (forsterite) | $Mg_2SiO_4$ | Orthorhombic | a = 4.7534; b = 10.1902; c = 5.9783 | Pnma (No 62) |
| Wadsleyite | $Mg_2SiO_4$ | Orthorhombic | a = 5.6983; b = 11.438; c = 8.2566 | Imma (No 74) |
| Ringwoodite | $Mg_2SiO_4$ | Cubic | a = 8.0649 | Fd-3 m (No 227) |

for Fe, 0.03% for Mn, <0.01% for Mg, <0.01% for Ca, <0.02% for Na, and <0.01% for K. Natural and synthetic material obtained from C.M. Taylor Company were used as mineral standards. The composition of olivine, wadsleyite, and ringoodite is expressed as fayalite (Fa) mol%. Fa has composition $Fe_2SiO_4$ and, therefore, represents the Fe-rich endmember.

MicroRaman spectroscopy has been performed with a JASCO NRS-1000 instrument at the NIPR, equipped with a charge-coupled device (CCD), using a 532 nm (green light) solid laser light. The spectral resolution was about 1 μm. The laser light was standardized with silicon, using a band maximum at 520.2 $cm^{-1}$. The Raman spectra were obtained after two accumulations using 20 s integration times.

A FEI Helios NanoLab 650 dual beam system (Field Emission—FE-SEM and focused ion beam—FIB) was used to prepare site-specific TEM samples by $Ga^+$ ion sputtering, with an ion beam accelerating voltage of 30 kV and a beam current of 3 nA. TEM has been performed with a Philips CM20 instrument, operated at 200 kV and equipped with a Nanomegas "Spinning Star" precession unit and an Oxford INCA x-sight EDS detector. Microdiffraction, i.e., with a nearly parallel incident beam focused on the specimen with a spot size in the range 10–50 nm, was performed to acquire a single-crystal zone-axis pattern (ZAP). A selected area aperture of around 8 μm in diameter was set to acquire a selected area electron diffraction (SAED) pattern, so that nearly the entire FIB sample area could be selected for SAED. Java electron microscopy simulator (JEMS) software was used for simulation of kinematical as well as dynamical electron-diffraction patterns (Stadelmann 2004). Theoretical structures used for JEMS simulation are given in Table 1. Both instruments are located at the Electron Microscopy for Materials Science (EMAT) laboratory of the University of Antwerp, Belgium.

## MICROSTRUCTURES

### Shock Veins in a L6 Ordinary Chondrite

The series A 09578 - A 09607 consists of about 30 paired ordinary chondrites collected in Antarctica during a joint Belgian–Japanese mission in the season 2009–2010 (Yamaguchi et al. 2014). During routine analyses for meteorite classification, shock veins and ringwoodite have been detected in many meteorites of the series, whereas the transformation of plagioclase in maskelynite was assumed by optical microscopy observations for all the samples. Sample A 09584 was selected for further studies, because it apparently contains the largest and most abundant ringwoodite grains in the whole series.

Shock veins are widespread in the sample (Fig. 1a). Shock veins are 100–200 μm wide and appear dark under transmitted light. They are located along grain or chondrule boundaries. The veins contain angular mineral and lithic clasts suspended in a matrix, which consists of fine-grained mineral clasts and olivine-ringwoodite microlites, ca. 10 μm in size, immersed in a solidified silicate melt (Figs. 1b and 1c). The coarse-grained clasts mostly consist of olivine and pyroxene. Some grains along the vein margin seem to have experienced incipient melting or intense shock for a few tens of micrometers from the contact with the vein. Olivine microlites in the matrix are preferentially concentrated along the clast margins, apparently having formed by epitactic growth and showing fine concentric zoning (Fig. 1d). Ringwoodite is generally localized at the margin of olivine clasts, but locally individual crystals of ringwoodite occur in the melt. Maskelynite is widespread in the sample, also in areas of the samples apparently not affected by shock veins. A few grains in the shock veins also consist of maskelynite. Pyroxene clasts in the shock veins display evidence of partial melting.

### Shocked Olivine Clasts

Olivine clasts are generally rimmed by a layer of ringwoodite, with thicknesses ranging from a few up to 50 μm (Figs. 1b–d). The core of such clasts contains a dense network of dark (in BSE-SEM images) lamellae and whitish domains. Locally, a few olivine grains protrude from the host into the shock vein. These grains also exhibit a ringwoodite rim and dark and whitish domains in the core, similarly to the core-and-rim structure observed in olivine clasts in the shock vein, but with a progressive increase in density of the whitish domains toward the shock vein.

Ringwoodite occurs also in individual grains with rounded shape and grain size ranging from 5 to 10 μm

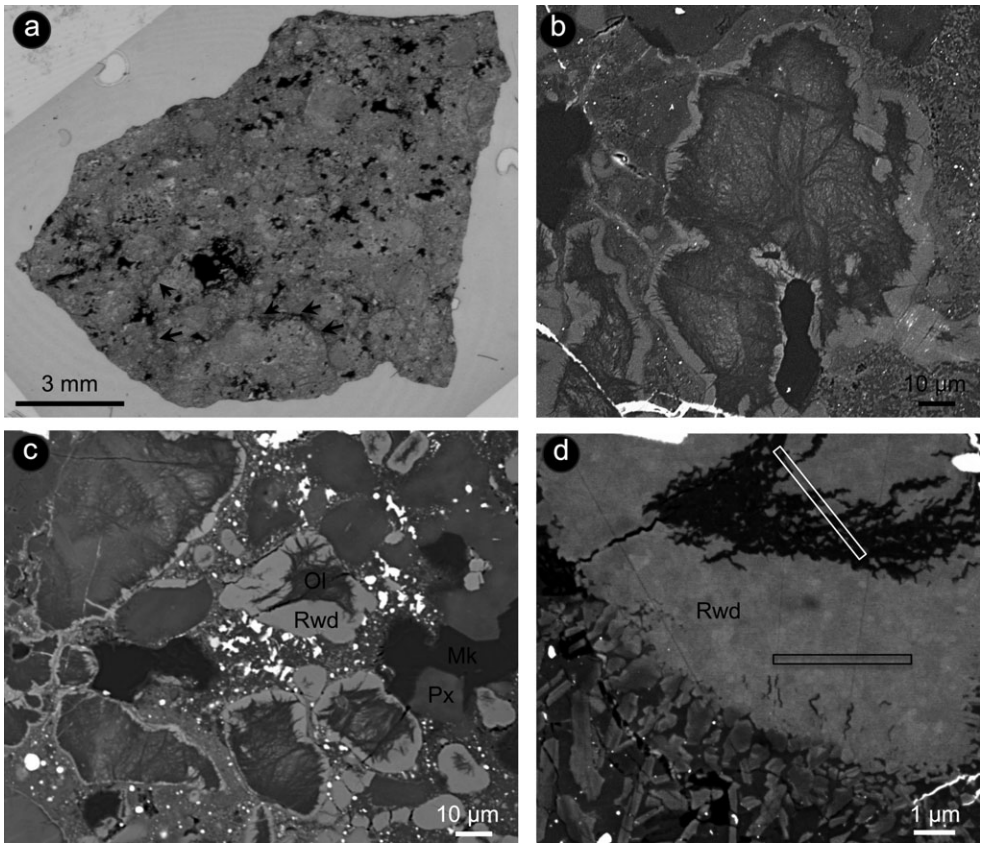


Fig. 1. Shocked olivine in A 09584, L6 ordinary chondrite recording shock stage S5-6. a) Polarized light image of a 35 μm—thick thin section of the sample. The occurrence of melt veins is marked with arrows. b) A clast of "olivine" in the shock vein with a rim of ringwoodite and a complex structure in the core. c) Clasts of olivine showing the same feature of (b). The thickness of the ringwoodite rim varies due to cut effect. d) Detail of the ringwoodite rim and of the internal olivine structure in a clast in the shock vein. Notice the olivine microlites that crystallize from the melt. In the figure, the areas where the transmitted electron microscopy (TEM) foils were cut with focus ion beam (FIB) are marked: the black box indicates the location in the ringwoodite rim and white box that in the core of the clast). Figure (b), (c), and (d) are backscattered electron (BSE) images.

(Fig. 1c). However, individual grains of ringwoodite might result from a 3-D sectioning effect due to sample preparation, where the only ringwoodite rim of olivine clasts has been exposed by polishing. The presence of ringwoodite is easily recognized by a brighter gray shade than the olivine, in backscattered electron (BSE) image, as a result of the different Mg/Fe ratio (lower in the ringwoodite than in the clast core). Raman spectroscopy has confirmed the occurrence of ringwoodite in the rim of olivine clasts (Fig. 2).

The core of shocked olivine clasts show a complex structure, with curved lamellae, 1–2 μm in thickness, organized in a dense network (Fig. 1b). The lamellae are immersed in a matrix that appears whitish in BSE images, suggesting higher Fe/Mg ratio than in the lamellae, which appear dark gray in BSE images. Raman spectra of this area show coexisting olivine and ringwoodite, with peaks of both phases (Fig. 2).

The correlation between Mg and Fe abundance between phases is shown in Fig. 3, with selected elemental maps obtained with the microprobe. The lamellae in the cores of the clasts have higher Mg content than the material in which they are immersed and then the ringwoodite rim, whereas the ringwoodite rim has a higher Fe content than the lamellae. The lamellae in the clast core seem to have the same Mg and Fe content as the unshocked olivine in the wall rock, in the upper left image. In this grain, partially in the shock vein, the occurrence of Fe-rich material between the lamellae increases toward the shock vein (Fig. 3) and the density of olivine lamellae decreases as well. A similar trend can be observed between the inner core and the rim of olivine–ringwoodite clasts.

## TEM INVESTIGATION

As some microstructural features are smaller than the resolution limit of Raman spectroscopy (1–2 μm), TEM investigations were performed on a selected

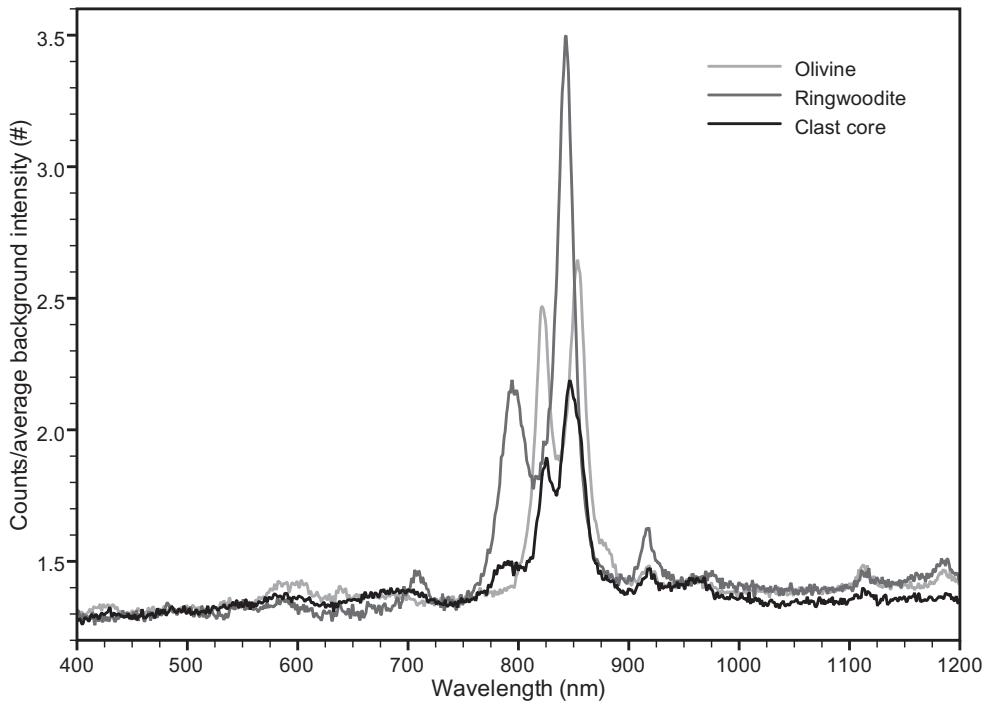


Fig. 2. Raman spectra of the situation showed in Fig. 1d. The characteristic spectrum of olivine was taken from a large grain in the matrix of the samples. The spectrum of ringwoodite was taken from a large rim of an olivine clast. The mixed spectrum was taken from the core of an olivine clast. In the latter, characteristic peaks of both olivine and ringwoodite are present. The counts ($y$-axis) are normalized over the average background intensity.

shocked olivine grain, shown in Fig. 1c. Two foils, on two selected locations, were prepared by Ga ion sputtering with a FIB instrument. The size of a foil is about 5 × 4 μm, with an average thickness of about 90 nm. The two selected locations are representative of both the ringwoodite rim of the chosen grain, to be used as reference material, and of the core of the grain, including the lamellae and the material in between. The investigated phase was identification by their diffraction pattern, because, as polymorphs, they might have the same composition but different crystal system and space group (Table 1). The different crystallographic symmetries, from olivine to ringwoodite, correspond to progressive increase in crystal density, therefore in pressure, which is also known in rocks from the Earth mantle (e.g., Agee 1998).

## Ringwoodite Rim

The foil cut in the ringwoodite rim reveals an inhomogeneous internal structure (Fig. 4a). The ringwoodite rim does not consist of a single crystal formed by epitactic growth, as suggested by the BSE–SEM images, but rather consists of an aggregate of tiny hypidiomorphic ringwoodite grains with average sizes of about 500 nm. The ringwoodite grains have prismatic shapes and exhibit a random orientation in the investigated section (Fig. 4b). Internally, ringwoodite grains have strain features that resemble stacking faults (Fig. 4c). The nature of these stacking faults was not determined, but the observed features are similar to those described by Madon and Poirier (1983), Xie and Sharp (2006), and Miyahara et al. (2008), although referred to different formation processes. The ZAP of an individual grain obtained by precession electron diffraction minimizing dynamical scattering is compared with the kinematical simulated pattern of the [001] zone of the ringwoodite structure showing good correspondence (Figs. 5a–c). The rings in the SAED pattern from the rim sample (Fig. 5d) can be explained both by ringwoodite and possibly a certain amount of wadsleyite, but no olivine is present (several olivine rings are missing). The absence of amorphous material is confirmed by the cumulative diffraction, as the pattern does not show any central diffuse rings.

## At the Clast Core

The foil from the core of the selected olivine grain has been cut normal to the network of ultra fine-grained dark lamellae in the whitish matrix, according to

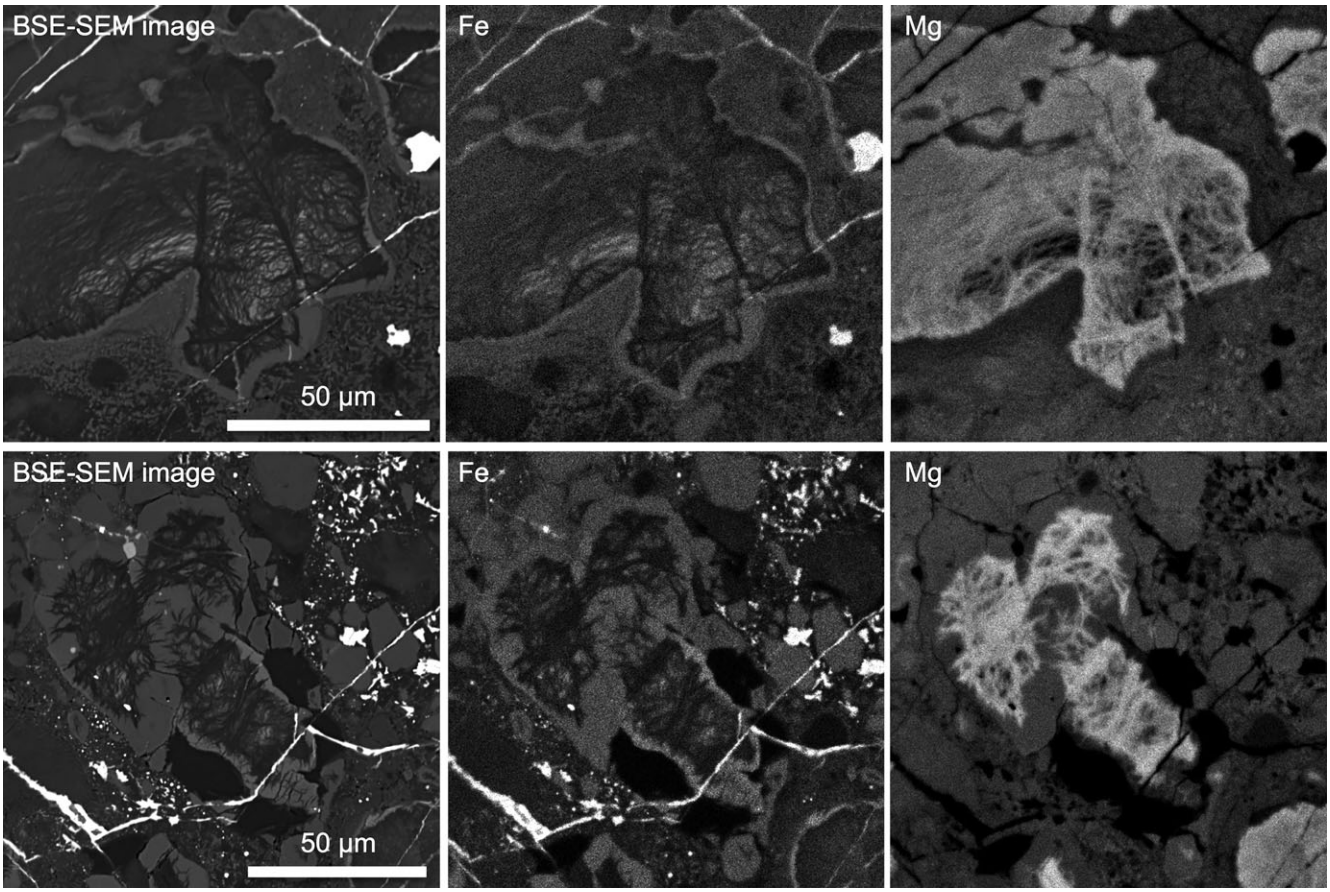


Fig. 3. Microprobe chemical maps of selected elements. Two clasts (upper and lower row) are chosen from the shock vein. The first example is an olivine grain detached from the wall rock. For each example, a BSE image and the map of the abundance of Fe and Mg are shown. In both clasts, the ringwoodite rim is enriched in Fe with respect to the core, which on the contrary has a complex structure, with Mg-rich lamellae and domains enriched in Fe.

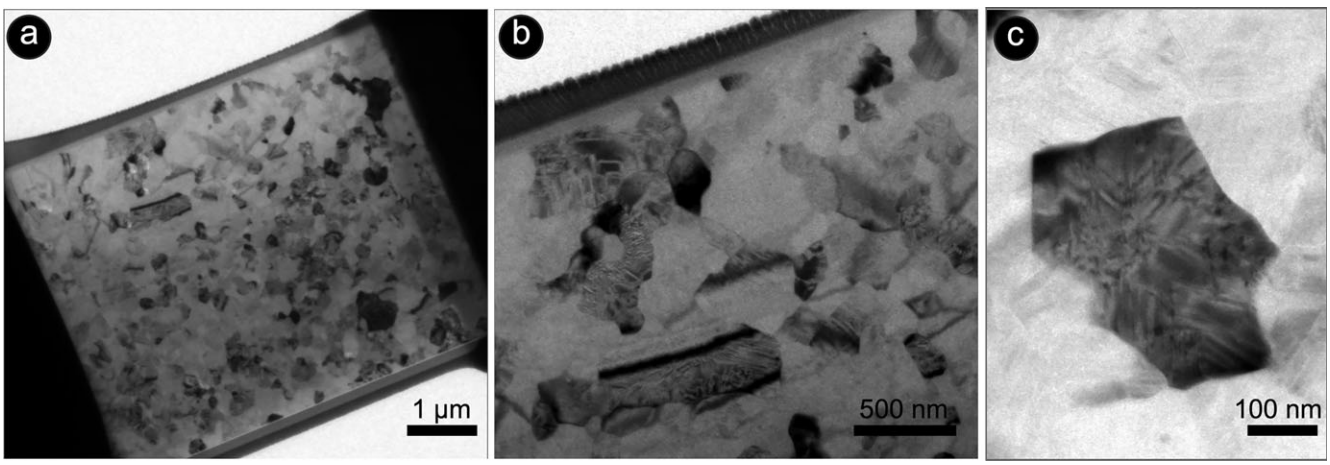


Fig. 4. TEM images from the rim of shocked clasts. a) TEM bright-field image of the FIB sample, showing that the ringwoodite rim consists of an aggregate of submicrometer grains. b) Detail of (a) showing defect features, possibly stacking faults, in the grains. c) A selected grain, full of internal features, at higher magnification.

BSE-SEM images (Fig. 1d). Unfortunately, the produced cross section contains only a few bright domains (Fig. 6a).

The TEM bright-field image shows a complex internal structure (Fig. 6b). What appeared as dark lamellae in BSE-SEM images actually consists of

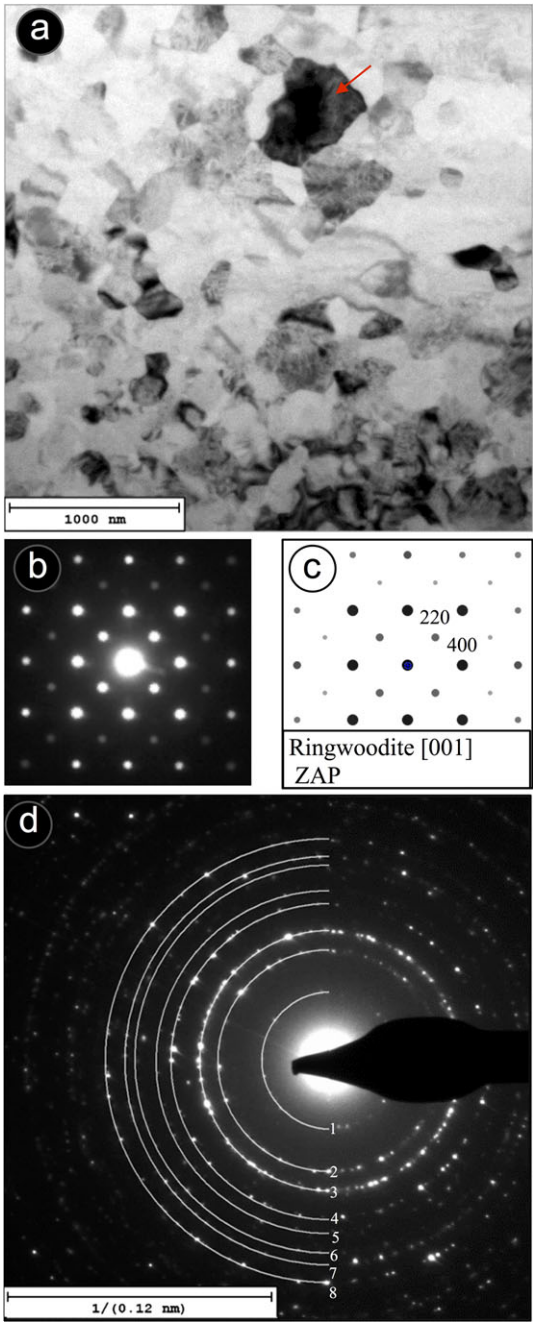


Fig. 5. TEM images from the rim of shocked clasts. a) TEM bright-field image of a limited area of Fig. 4a. The selected grain for diffraction is marked with a red arrow. b) Experimental zone-axis pattern (ZAP) of the selected grain and the corresponding simulated [001] ZAP of ringwoodite (c). d) Selected area electron diffraction (SAED) ring patterns of the whole FIB foil from the rim. Rings overlapped on the experimental patterns were identified and indexed (see Table 2 and text for more details).

domains containing nanocrystals (~150 nm in width, but often up to 1 μm in length) with a strong shape preferred orientation. These nanocrystals have a prismatic shape, with an apparent aspect ratio of 3:1, and seem to be aligned parallel to the field of view (Fig. 6c). The whitish material between the lamellae in BSE–SEM images consists of veinlets with an irregular shape and maximum thickness of ~500 nm, which crosscut the aggregate of iso-oriented nanocrystals (Figs. 6b and 6c). By tilting the sample in bright-field conditions these veinlets are seen to consist of nanocrystals, which are less than 200 nm in size and apparently have random orientation (Fig. 6d). The nanocrystals in the veinlets are full of crystallographic defects, similar to those observed in the ringwoodite grains in the clast rim.

Due to the small dimensions of the crystals in the clast core, no precession electron diffraction could be applied. As a result and due to the similarity of the different unit cells of the possible structures, neither individual, single zone diffraction patterns nor SAED ring patterns allow a clear identification of the phases in the core. As seen from the measured a/b ratios (standard deviation 0.05), the dimensions measured from the ZAP in Fig. 7a obtained from the grain encircled in Fig. 5c can be explained by the [210] olivine pattern, while those in Fig. 7c, obtained from the grain indicated by the arrow in Fig. 6c, can be explained by that of [411] olivine or [001] wadsleyite. In this case, dynamical diffraction patterns have been calculated since no precession was used, resulting in the observation of cinematically forbidden reflections.

Similar conclusions can be obtained from SAED patterns from the whole investigated foil. The ring pattern obtained from the clast core (Fig. 8; Table 2) clearly shows the existence of olivine (some rings can only be explained by this structure). Also wadsleyite could be present but for ringwoodite too many rings are missing. Even in this case, the absence of amorphous material is confirmed by the lack of any central diffuse rings.

EDS analyses of several grains in the foil have been performed to correlate the compositional variations marked by the BSE–SEM images with the crystallographic identification of the different phases. As suggested by the BSE images, the iso-oriented grains (dark lamellae in BSE-SEM images) exhibit high Mg/Fe ratio, whereas the grains in the veinlets (bright domains in BSE-SEM images) exhibit low Mg/Fe ratio, but there is a wide range of intermediate compositions (Fig. 9).

## DISCUSSION

### Identification of Phases by Their Composition and Diffraction

Microprobe investigations on olivine clasts in the shocked vein have revealed a large compositional variability (Table 3). In Fig. 9, the Fa content of four

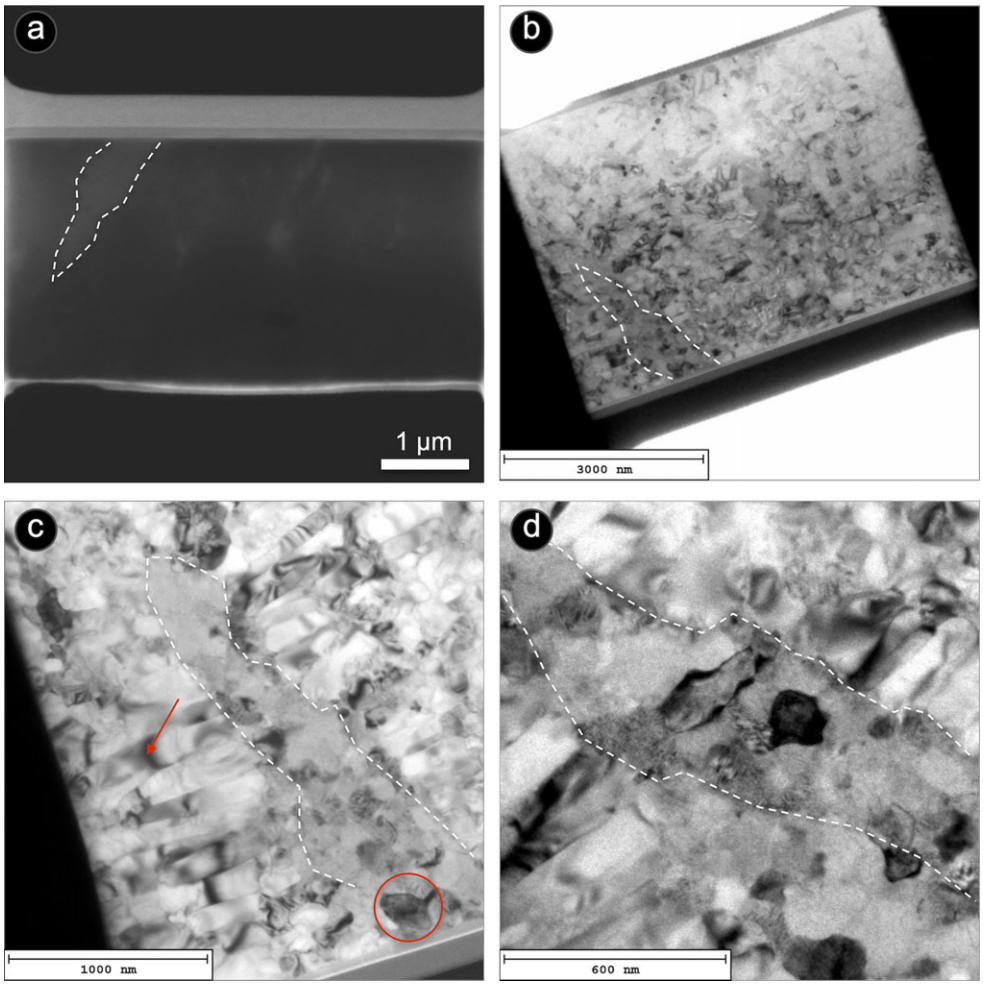


Fig. 6. TEM images from the core of the shocked clasts. a) BSE image of the TEM sample cut with the FIB. The bright veinlet is marked with a white dashed line. b) TEM bright-field image of the same sample. The area marked with a dashed line corresponds to that in (a) and is used as orientation reference. c) Detail of the veinlet and the host material. Note the aligned grains on the lower left corner of the image. The arrow and the circle mark the grains selected for diffraction and showed in Fig. 7. d) A closer look to the internal structure of the veinlet, with submicrometer grains with internal defect features.

olivine grains from relict chondrules, not affected by the shock metamorphism and far enough from the shock veins, is plotted as reference. The Fa content in the chondrule olivine is consistent among samples ($Fa_{24}$), with negligible variations. The lamellae that appear dark gray in BSE-SEM images in the core of the clasts show a broader range of Fa contents, from equal to that in chondrules to much lower (~$Fa_{10}$). The ringwoodite rim displays a broad range of Fa contents as well, but clearly with a higher Fa content ($Fa_{37\text{-}55}$) than that in the chondrules. Nevertheless, the Fa content in ringwoodite has a clear gap with respect to the other two phases. The Fa content of the domains in the clast core, where the dark lamellae and the bright material, as observed with the BSE-SEM images, form a dense network, seems to fall within this compositional gap. This might be due to the spatial resolution of the microprobe, which is unable to distinguish phases smaller than 1–2 μm. The result is a mixed composition between the dark and the bright domains in BSE. For comparison, also the TEM-EDS analyses on selected crystals of the foil cut within the clast core are plotted. Despite the fact that EDS can provide only qualitative analyses of the investigated species, the small spot size in the TEM limits spurious radiation from neighboring crystals. The range of Fa content is very broad and includes all the compositional variations observed at the microprobe, but the compositional gap between the dark domains in olivine clasts and the ringwoodite is confirmed. This suggests that the composition of the bright domain in BSE images (veinlets in the TEM bright-field image) is enriched in Fe and, therefore, is close to that of the ringwoodite rim. On the other hand, the dark lamellae in BSE images (iso-oriented crystals in

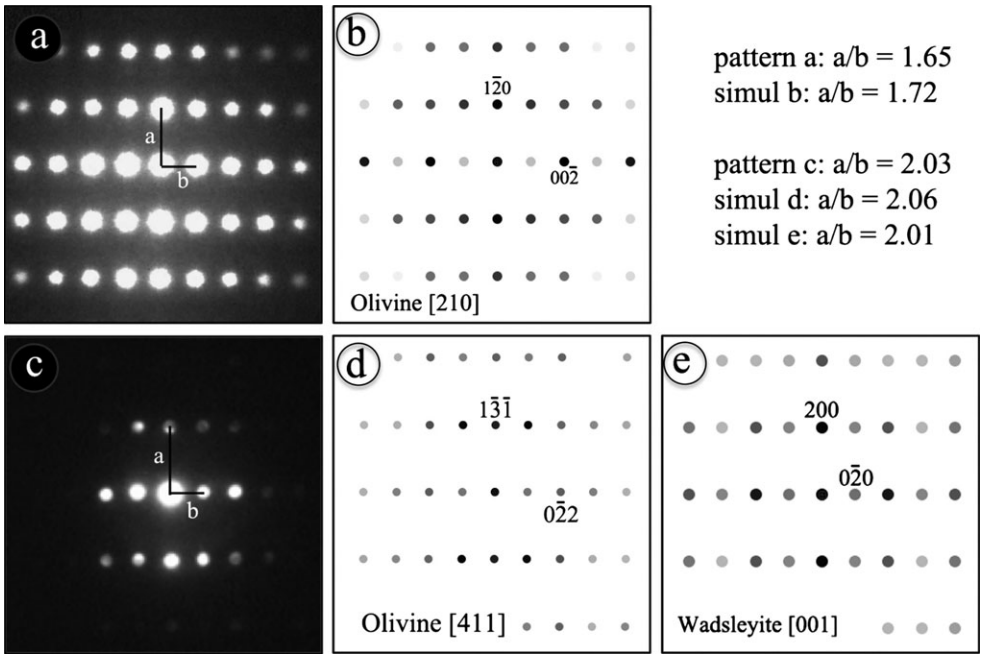


Fig. 7. Diffraction patterns of grains in the clast core. a) Experimental ZAP of the grain encircled in Fig. 6c in the veinlet. b) Dynamically simulated [210] ZAP of the olivine phase corresponding to (a). c) Experimental ZAP of the grain marked with an arrow in Fig. 5c in the iso-oriented domain and corresponding dynamically simulated [411] and [001] ZAPs of the olivine (d) and wadsleyite (e), respectively. The measured a/b ratios are also listed (±0.05).

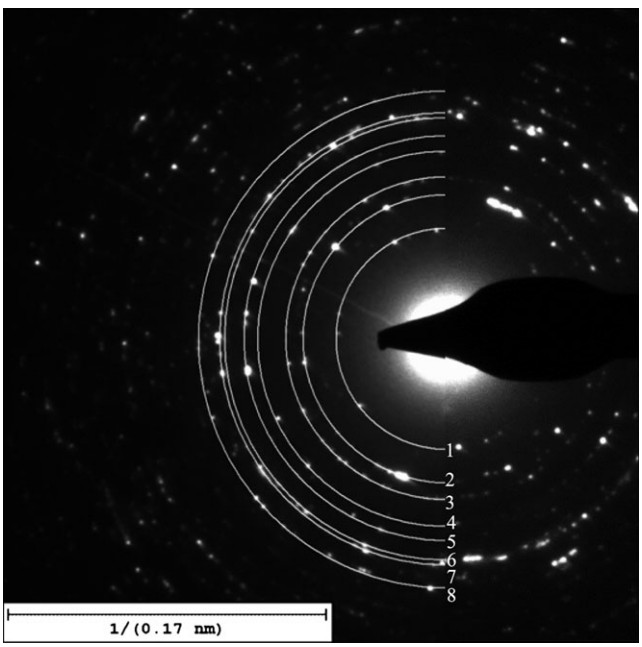


Fig. 8. SAED ring patterns of the FIB samples obtained from the clast core. Rings overlapped on the experimental patterns were identified and indexed (see Table 2 and text for more details).

the TEM bright-field image) have compositions that range from the same to Mg-enriched members than the unshocked olivine in the same sample.

Table 2. *d* distance (nm) of the indexed rings from the selected area electron diffraction (SAED) patterns that are shown in Fig. 5d and 8 and that, respectively, correspond to the rim and the core of the investigated shocked olivine grain, and related *hkl* of the different phases taken into consideration.

| | SAED in the grain rim | | | SAED in the grain core | | | |
|---|---|---|---|---|---|---|---|
| Ring | *d* distance | Rwd *hkl* | Wds *hkl* | *d* distance | Ol *hkl* | Wds *hkl* | Rwd *hkl* |
| 1 | 0.46 | 111 | 101 | 0.498 | 020 | 110 | – |
| 2 | 0.29 | 220 | 040 | 0.380 | 101 | – | – |
| 3 | 0.24 | 113 | 141 | 0.337 | 030 | 022 | – |
| 4 | 0.2 | 400 | 004 | 0.292 | 012 | 040 | 220 |
| 5 | 0.18 | 331 | 242 | 0.269 | 022 | 013 | – |
| 6 | 0.16 | 422 | 224 | 0.244 | 112 | 141 | 113 |
| 7 | 0.155 | 333 | 125 | 0.242 | 200 | – | – |
| 8 | 0.14 | 440 | 064 | 0.219 | 211 | 222 | – |

The following mineral abbreviations, according to Whitney and Evans (2010), are used: Rwd for ringwoodite, Wds for wadsleyite, and Ol for olivine.

The identification of the different phases of olivine composition in the shocked sample, as the ultra fine-grain size, is suitable by electron diffraction. For the ringwoodite rim the presence of ringwoodite is confirmed, the occurrence of wadsleyite is improbable but the presence of melt is very unlikely (Fig. 5d).

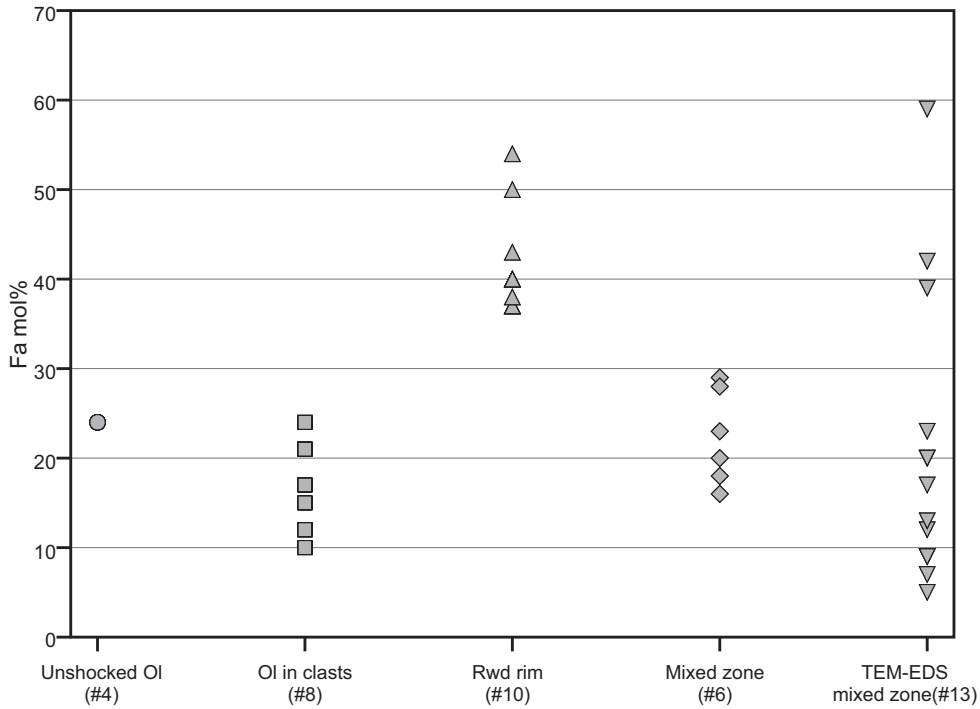


Fig. 9. Chemical variability in the investigated phases expressed as Fa content. The Fa content has been calculated on EMPA analysis except for the last series, where EDS analyses at TEM were considered for comparison. The approximation to 100% and the lack of standards is compensated in the EDS analyses by the possibility to focus on ultra fine-grained crystals. (Unshocked Ol = olivine in chondrules far from the shock vein, Ol in clasts = dark domains at the core of olivine clasts, Rwd rim = composition in the ringwoodite rim, mixed zone = analyses in the core of olivine clasts, where dark and bright domains are present, TEM-EDS mixed zone = EDS analyses focused on individual grains of the dark and bright domains in the core of olivine clasts; the number of analysis is given in brackets.)

Table 3. Composition of selected phases within olivine clasts in shock veins, as analyzed by electron microprobe. Data are given in wt%, except when indicated.

| | Olivine (avg #8) | St.dev. | Ringwoodite (avg #11) | St.dev. | Interm. (avg #3) | St.dev. |
|---|---|---|---|---|---|---|
| $SiO_2$ | 40.28 | 1.00 | 36.85 | 0.92 | 38.21 | 0.44 |
| $TiO_2$ | bdl | – | bdl | – | bdl | – |
| $Al_2O_3$ | bdl | – | 0.24 | 0.11 | bdl | – |
| $Cr_2O_3$ | 0.03 | 0.01 | 0.05 | 0.04 | bdl | – |
| FeO | 15.78 | 4.55 | 35.92 | 3.89 | 26.53 | 0.84 |
| MnO | 0.36 | 0.12 | 0.07 | 0.04 | 0.41 | 0.06 |
| MgO | 44.62 | 4.02 | 28.04 | 3.28 | 36.05 | 0.88 |
| CaO | 0.04 | 0.05 | 0.05 | 0.02 | 0.02 | 0.01 |
| $Na_2O$ | 0.01 | 0.01 | 0.03 | 0.02 | 0.01 | 0.01 |
| $K_2O$ | bdl | – | bdl | – | bdl | – |
| Total | 101.15 | | 101.28 | | 101.25 | |
| Fa (mol%) | 17 | 5 | 42 | 6 | 26 | 5 |

avg = average; st.dev. = standard deviation; interm. = intermediate, area with unknown lamellae in a whitish (under BSE) groundmass; bdl = below detection limit; Fa = fayalite.

In the core of olivine clasts, the fine-grained aggregate is difficult to interpret. The occurrence of olivine is confirmed by TEM diffraction, the presence of wadsleyite is very probable, but there is no evidence of the presence of ringwoodite or amorphous phase-glass (Figs. 7 and 8; Table 2). Considering in detail the different phases, the dark lamellas that are visible in BSE-SEM images correspond to iso-oriented nanocrystals of olivine or wadsleyite, both interpretations are possible, with a general Mg-rich composition. The bright areas between the lamellae in BSE–SEM images correspond to veinlets of randomly

arranged nanocrystals of olivine. The occurrence of olivine in the veinlets, rather than wadsleyite, is also supported by the high Fe content. Nevertheless, only a few crystals in the veinlets could be analyzed by TEM diffraction because limited positions of reflections could be taken into account.

## Peak Pressure Estimate

The occurrence of high-pressure phases in shock veins has been used for shock pressure estimates since their discovery. The most widely used calibration is that established in Stöffler et al. (1991). The presence of maskelynite is referred to a shock pressure higher than 35 GPa, whereas the occurrence of ringwoodite further increases the minimum shock pressure to 55 GPa. Sharp and DeCarli (2006) showed the limitations of this calibration. The type of experiments and the unawareness of local phenomena that affect the shock wave intensity have probably led to an overestimate of the shock pressure related to the formation of such phases. In particular, the appearance of maskelynite is referred to shock pressure as low as 20–25 GPa in preheated samples and only slightly higher for samples at room temperature. According to experiments by Fritz et al. (2011), the shock pressure for transformation into maskelynite depends also on the original composition of plagioclase, from ~30 GPa for albitic terms to ~20 GPa for anorthitic members. In A 09584 the presence of maskelynite was deduced only by optical observations, neither verified by Raman spectroscopy, nor by TEM. Gillet et al. (2000) described an aggregate of nanocrystals of hollandite that with the optical microscope appears very similar to maskelynite, because of the ultra fine-grain size of the crystals. The transformation of plagioclase into hollandite would provide a different shock pressure estimate, between 12 and 24 GPa. The shock pressure necessary for the transformation of plagioclase into hollandite is also correlated with initial composition of plagioclase. The formation of ringwoodite involves a complex process that is discussed in the following section, but in any case the transformation of olivine into ringwoodite was experimentally reproduced at lower pressure than in Stöffler's calibration, e.g., at about 16 GPa in static experiments at 900 °C by Kerschhofer et al. (1998) and higher than 18 GPa but with a strong dependence on temperature and on duration of the shock pulse, according to Sharp and DeCarli (2006). Thus, individual high-pressure phases in A 09584 are stable at pressure not exceeding ca. 24 GPa (e.g., Xie et al. 2006).

This introduces a further issue of the estimate of the shock pressure, which is the duration of the process that caused the formation of ringwoodite. In A 09584, the formation of all the observed features must have occurred in a relatively short time range, because of the transient nature of an impact event. However, according to the modeling of the thermal evolution of shock veins by Shaw and Walton (2013), the shock pulse in chondrites is quite long (approximately 1 s). In the case of thin shock veins, the shock pulse exceeds the quench time and, therefore, the phases that crystallize in this time range have recorded the shock peak pressure. Sharp and DeCarli (2006) show that pressure equilibrium can be reached in nanoseconds, even in heterogeneous material. This suggests that the investigated high-pressure phases in A 09584 may have recorded the shock pressure of the compression stage of the impact event before quenching.

However, the correlation between the crystallization of some phases and the peak pressure is straightforward only for phases crystallized from the impact melt, but is more complex for phases formed by solid-state transformations processes, because their formation requires exceeding pressure to activate nucleation (Sharp and DeCarli 2006). Therefore, understanding the formation process of the high-pressure phases becomes fundamental for any interpretation of the impact event.

## Formation Process of the Observed Shock Features

The transformation of olivine into ringwoodite along the grain boundaries is very likely a solid-state process, by heterogeneous nucleation at grain boundaries of the host olivine, consistently with interpretations in Xie and Sharp (2006) and Xie et al. (2012). Miyahara et al. (2008) proposed that aggregate of olivine and wadsleyite could form by fractional crystallization from olivine melt, suggesting that wadsleyite crystallization anticipates the formation of ringwoodite at lower temperature and from Mg-depleted melt. According to this hypothesis, crystallization from a molten olivine should have first produced epitactic Mg-rich wadsleyite and only after a certain time the melt would have been enriched in Fe, resulting in a layered structure that was not observed in the olivine clasts in A 09584. Nevertheless, this process likely occurred in the formation of microlites with olivine composition that have crystallized in the melt, where a fine-grained zoning with a dark gray core and a bright gray rim are observed in BSE images (Fig. 1d).

The investigated ringwoodite crystals contain stacking faults (Fig. 4). Although the occurrence of stacking faults is generally referred to crystallization from a melt, as results of growth defects (e.g., Sharp et al. 1997), similar arrangement of stacking faults has been reported also in polycrystalline aggregates of ringwoodite, which likely formed by solid-state

transformation (Xie and Sharp 2006). On the other hand, stacking faults were observed also in ringwoodite in a wadsleyite-ringwoodite aggregate, which was interpreted as the result of segmentation of a zoned grain that formed by fractional crystallization from an olivine melt (Miyahara et al. 2008). According to these authors, stacking faults are due to the stress induced by the deformation of the crystals during segmentation and rearrangement. This process very unlikely to have occurred in the investigated olivine clasts in A 09584, where the transformation into ringwoodite occurred in situ and involved a larger area than that described by Miyahara et al. (2008). In addition, there is no evidence of local shear deformation and mixing between high-pressure phases. Two types of stacking faults have been found in wadsleyite in the Peace River meteorite and were interpreted as (i) inherited from the original phase in the core of the grains and (ii) as result of local high stress at the grain boundaries, suggesting incipient transformation into ringwoodite (Price 1983). Madon and Poirier (1983) suggested that the presence of twin-boundary-like defects in wadsleyite is indicative of growth from a melt. Stacking faults in ringwoodite in A 09584 were not investigated in detail, but their occurrence suggests local stress conditions, which might be related to lattice adjustment in the polymorphic transformation, due to the fast and not-at-equilibrium shock process. Ringwoodite is observed only in contact with the shock melt. This is interpreted as a favorable situation for the olivine-ringwoodite transformation, as the shock melt likely provided the high temperature necessary for the activation of the process and the diffusion of Fe and Mg, resulting in the different composition of ringwoodite with respect to the original olivine (Xie and Sharp 2006).

Therefore, the formation of the ringwoodite rim in our sample is consistent with the hypothesis of solid-state transformation, by heterogeneous nucleation along olivine boundary. As the ringwoodite rim has a higher Fa content, the transformation was likely controlled by diffusion under shock-induced, high-temperature conditions (Sharp and DeCarli 2006; Xie et al. 2012).

Nevertheless, the complex features observed at the core of the shocked clasts, characterized by both compositional and phase variability, require a more complex and comprehensive explanation. The olivine veinlets in the clast core cannot be explained by simple intracrystalline nucleation and growth, like those described by Kerschhofer et al. (1998), because high-pressure polymorphs at the place of olivine should have formed.

The shock veins that host the shocked clasts of olivine formed most likely by shock melting of the rock during the compressional stage, as experimentally demonstrated by Kenkmann et al. (2000). These veins are not planar but are rather localized along grain boundaries. This is against a possible origin by friction along a shear plane. In addition, there is no evidence of any slip along the surfaces. The formation of high-pressure polymorphs should, therefore, also be related to the compression stage.

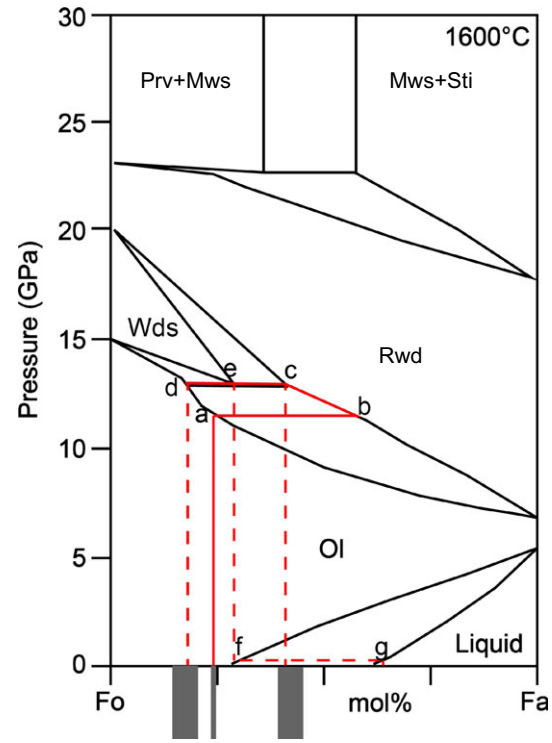


Fig. 10. Pressure-composition phase diagram for temperature of 1600 °C, after Agee (1998). The red line represents our interpretation of the phase evolution, see text for explanation. The gray boxes at the bottom represent the composition of the investigated phases as in Fig. 9, with the respective standard deviation. (Fo = forsterite; Fa = fayalite; Ol = olivine; Rwd = ringwoodite; Wds = wadsleyite; Prv = perovskite; Mws = magnesio-wüstite; Sti = stishovite.) Mineral abbreviations according to Whitney and Evans (2010).

As shown above, pressure equilibrium is achieved rapidly at the crystal scale (Sharp and DeCarli 2006) and the shock pulse in chondrites is considered long enough for diffusion-controlled crystallization (Shaw and Walton 2013). This legitimates the use of a pressure-composition phase diagram, on the local scale of the single grain, assuming local equilibrium and static conditions for the duration of the shock pulse. The pressure-composition phase diagram that fits better with our observations is that one calculated for an ambient temperature of 1600 °C (after Agee 1998 and Mitra 2004). In Fig. 10, we show a theoretical path that could explain the features observed in A 09584. From the starting composition, corresponding to the Fa content in unshocked olivine in the sample, a sudden

increase in pressure (point a) due to an impact event triggers the nucleation of ringwoodite of composition as in point b. The original olivine and the newly formed ringwoodite change the respective compositions by diffusion until point d and c, where the pressure is high enough to form also wadsleyite. An alternative interpretation is that point e was immediately reached, with simultaneous nucleation of both ringwoodite and wadsleyite of the respective compositions, which are consistent with those measured in the sample. The hypothesis of the formation of ringwoodite prior to wadsleyite may be supported by the occurrence of ringwoodite exclusively along the clast rim, pointing to different processes of nucleation for the two polymorphs (i) heterogeneous nucleation along grain boundaries, in contact with the melt, for the ringwoodite and (ii) intracrystalline heterogeneous nucleation along crystallographic planes or perhaps incipient discontinuities, such as planar fractures in olivine. Whatever path has been followed up to point e, the process must have occurred during the compression stage. The combination of composition and crystallographic identification of the phases present in the clasts, according to the pressure-phase diagram at certain temperature, might be used as shock-barometer for the equilibration pressure in the compression stage at the grain scale, although pressure and temperature cannot be obviously constrained in the investigated sample. As previously discussed, this shock-barometer can provide only a lower limit of the peak pressure, because it does not account for the activation energy required for nucleation. The resulting shock pressure would be about 13 GPa for minimum 1600 °C temperature, but very likely a combination of higher pressure and lower temperature might also be consistent with the coexistence of the observed phases. However, the shock pressure estimated by the mineral paragenesis is much lower than that expected according to the correlation by Stöffler et al. (1991).

On the other hand, the formation of the olivine veinlets with high Fe content occurred in a later stage of the shock event, possibly due to the release of pressure. The compression stage is followed by sudden pressure unloading, called release wave (French 1998). The shock release might have triggered the formation of cracks in the core of the olivine clasts and some olivine underwent adiabatic melting (point f in Fig. 10). The first drop of melt would have had composition corresponding to point g (even more Fe rich than the ringwoodite), which crystallized as olivine during the fast cooling to the ambient temperature and consistently with the ambient pressure conditions. This might explain the Fe-rich compositions of some grains of olivine in the whitish veinlets (in BSE-SEM images) in the clast core, as detected by TEM-EDS. Ringwoodite and wadsleyite were probably not affected by this late stage because they already formed at much higher pressure and the shock release and the subsequent temperature drop was fast enough to preserve these phases by retrogression, although metastable under the new ambient conditions. Other pressure-composition phase diagrams produced by Agee (1998), obtained for different temperatures, were considered, but none of them is fully consistent with our observations.

## CONCLUSIONS

Shocked olivine clasts are widespread in shock veins crosscutting sample A 09584, a L6 ordinary chondrite, with shock stage S5-6, collected in Antarctica. These olivine clasts generally present a complex structure, with an aggregate of ringwoodite nanocrystals rimming a core that consists of a dense network of dark lamellae (in BSE-SEM images) with bright domains in between. Investigations with microprobe and TEM have allowed the identification of the phases occurring in the clasts; ringwoodite with high Fe content is limited to the rim, the lamellae in the core consist of high Mg, iso-oriented nanocrystals of olivine and wadsleyite, and the bright domains in BSE-TEM images are actually veinlets crosscutting the lamellae and consisting of nanocrystals of olivine that are highly enriched in Fe. The coexistence of all these phases can be explained by a pressure-composition phase diagram, calculated for high-temperature conditions. The ringwoodite in the grains' rim and the wadsleyite/olivine iso-oriented crystals likely formed by shock-induced solid-state phase transformation, under high-temperature conditions and diffusion-controlled heterogeneous nucleation. The veinlets of olivine in the clast cores might have originated by late crystallization of a melt, which formed by shock release, following the compression stage, along cracks in the core of olivine clasts.

*Acknowledgments*—The authors thank S. Ozawa for assistance with Raman spectroscopy at the National Institute of Polar Research, Tachikawa, Japan; S. Van Den Broeck for the FIB cut at EMAT, Antwerp, Belgium; and S. McKibbin (VUB) for the insightful discussions on phase diagrams and interpretation. LP was funded by the Belgian Science Policy Office (BELSPO). G. Ji was supported by the FWO project G.0603.10N. The sample, a polished thin section, was kindly provided by the NIPR. This research is supported by the BELAM project and the Interuniversity Attraction Poles Programme Planet Topers both financed by the BELSPO. R. Wirth and C. Koeberl are thanked for helpful comments in

reviewing the paper. A. Greshake and J. Fritz are thanked for insightful discussions on the interpretation of the observed features in the framework of impact events. C. Koeberl is also thanked for editorial handling of the manuscript.

*Editorial Handling*—Dr. Christian Koeberl

## REFERENCES

Agee C. B. 1998. Phase transformations and seismic structure in the upper mantle and transition zone. *Reviews in Mineralogy and Geochemistry* 37:165–203.

Chen M., El Goresy A., and Gillet P. 2004. Ringwoodite lamellae in olivine: Clues to olivine–ringwoodite phase transition mechanisms in shocked meteorites and subducting slabs. *Proceedings of the National Academy of Sciences* 101:15,033–15,037.

Feng L., Lin Y., Hu S., Xu L., and Miao B. 2011. Estimating compositions of natural ringwoodite in the heavily shocked Grove Mountains 052049 meteorite from Raman spectra. *American Mineralogist* 96:1480–1489.

French B. M. 1998. Traces of catastrophe—A handbook of shock-metamorphic effects in terrestrial meteorite impact structures. LPI Contribution 954. Houston, Texas: Lunar and Planetary Institute. 120 p.

Fritz J., Wünnemann K., Greshake A., Fernandes V. A. S. M., Boettger U., and Hornemann U. 2011. Shock pressure calibration for lunar plagioclase (abstract #1169). 42nd Lunar and Planetary Science Conference. CD-ROM.

Gillet P., Chen M., Dubrovinsky L., and El Goresy A. 2000. Natural $NaAlSi_3O_8$-hollandite in the shocked Sixiangkou meteorite. *Science* 287:1633–1636.

Greshake A., Fritz J., and Böttger U. 2011. Ringwoodite in the Martian shergottite Dar al Gani 670: The role of shearing (abstract #1092). 42nd Lunar and Planetary Science Conference. CD-ROM.

Kenkmann T., Hornemann U., and Stöffler D. 2000. Experimental generation of shock-induced pseudotachylites along lithological interfaces. *Meteoritics & Planetary Science* 35:1275–1290.

Kerschhofer L., Dupas C., Liu M., Sharp T. G., Durham W. B., and Rubie D. C. 1998. Polymorphic transformations between olivine, wadsleyite and ringwoodite: Mechanisms of intracrystalline nucleation and the role of elastic strain. *Mineralogical Magazine* 62:617–638.

Langenhorst F. 2002. Shock metamorphism of some minerals: Basic introduction and microstructural observations. *Bulletin of the Czech Geological Survey* 77:265–282.

Madon M. and Poirier J. P. 1983. Transmission electron microscope observation of α, β, and γ $(Mg, Fe)_2SiO_4$ in shocked meteorites: Planar defects and polymorphic transitions. *Physics of the Earth and Planetary Interiors* 33:31–44.

Mitra S. 2004. *High pressure geochemistry and mineral physics: Basics for planetology and geo-material science*. Amsterdam: Elsevier. 1272 p.

Miyahara M., El Goresy A., Ohtani E., Nagase T., Nishijima M., Vashaei Z., Ferroir T., Gillet P., Dubrovinsky L., and Simionovici A. 2008. Evidence for fractional crystallization of wadsleyite and ringwoodite from olivine melts in chondrules entrained in shock-melt veins. *Proceedings of the National Academy of Sciences* 105:8542–8547.

Miyahara M., Ohtani E., Kimura M., El Goresy A., Ozawa S., Nagase T., Nishijima M., and Hiraga K. 2010. Coherent and subsequent incoherent ringwoodite growth in olivine of shocked L6 chondrites. *Earth and Planetary Science Letters* 295:321–327.

Price G. D. 1983. The nature and significance of stacking faults in wadsleyite, natural β-$(Mg, Fe)_2SiO_4$ from the Peace River meteorite. *Physics of the Earth and Planetary Interiors* 33:137–147.

Sharp T. G. and DeCarli P. S. 2006. Shock effects in meteorites. In *Meteorites and the early solar system*, edited by Lauretta D. S. and McSween H. Y. Jr. Tucson, Arizona: The University of Arizona Press. pp. 653–678.

Sharp T. G., Lingemann C. M., Dupas C., and Stöffler D. 1997. Natural occurrence of $MgSiO_3$-ilmenite and evidence for $MgSiO_3$-perovskite in a shocked L chondrite. *Science* 277:352–355.

Shaw C. S. J. and Walton E. 2013. Thermal modeling of shock melts in Martian meteorites: Implications for preserving Martian atmospheric signatures and crystallization of high-pressure minerals from shock melts. *Meteoritics & Planetary Science* 48:758–770.

Smyth J. R. and Bish D. L. 1988. *Crystal structures and cation sites of the rock-forming minerals*. Boston: Allen and Unwin. 332 p.

Stadelmann P. A. 2004. JEMS (Java version of electron microscopy software). http://cimewww.epfl.ch/people/stadelmann/jemsWebSite/jems.html. Accessed March 18, 2014.

Stöffler D. and Langenhorst F. 1994. Shock metamorphism of quartz in nature and experiment: I basic observation and theory. *Meteoritics* 29:155–181.

Stöffler D., Keil K., and Scott E. R. 1991. Shock metamorphism of ordinary chondrites. *Geochimica et Cosmochimica Acta* 55:3845–3867.

Walton E. L. 2013. Shock metamorphism of Elephant Moraine A79001: Implications for olivine–ringwoodite transformation and the complex thermal history of heavily shocked Martian meteorites. *Geochimica et Cosmochimica Acta* 107:299–315.

Whitney D. L. and Evans B. W. 2010. Abbreviations for names of rock-forming minerals. *American Mineralogist* 95:185–187.

Xie Z. and Sharp T. G. 2006. Ringwoodite lamellae in olivine from the L6 S6 chondrite Tenham: constraints on the transformation mechanism (abstract #2306). 37th Lunar and Planetary Science Conference. CD-ROM.

Xie Z., Sharp T. G., and DeCarli P. S. 2006. High-pressure phases in a shock-induced melt vein of the Tenham L6 chondrite: Constraints on shock pressure and duration. *Geochimica et Cosmochimica Acta* 70:504–515.

Xie Z., Li X., Sharp T. G., and De Carli P. S. 2012. Shock-induced ringwoodite rims around olivine fragments in melt vein of Antarctic chondrite GRV 022321: Transformation mechanism (abstract #2776). 43rd Lunar and Planetary Science Conference. CD-ROM.

Yamaguchi A., Pittarello L., Kimura M., and Kojima H. 2014. *Meteorite Newsletter 23*. Tokyo: NIPR.